Diagnosis of Fatty Liver Disease by a Bright, Multiphoton-Active and Lipid-Droplet-Specific AIEgen with Nonaromatic Rotors

Hojeong Park,[a,b]+ Shijie Li,[c]+ Guangle Niu,[a,b,d]+ Haoke Zhang,[a,b] Zhuoyue Song,[c] Qing Lu,[d] Jun Zhang,[a] Chao Ma,[e] Ryan T. K. Kwok,[a,b] Jacky W. Y. Lam,[a,b] Kam Sing Wong,[e] Xiaoqiang Yu,[d] Qingping Xiong*[c,f] and Ben Zhong Tang*[a,b,g]

[a] H. Park, Prof. G. Niu, Dr. H. Zhang, Prof. Jun Zhang, Dr. R. T. K. Kwok, Dr. J. W. Y. Lam, Prof. B. Z. Tang
Department of Chemistry, The Hong Kong Branch of Chinese National Engineering Research Center for Tissue Restoration and Reconstruction, Institute for Advanced Study, State Key Laboratory of Neuroscience, Division of Life Science and Department of Chemical and Biological Engineering, The Hong Kong University of Science and Technology, Clear Water Bay, Kowloon, Hong Kong 999077, China
E-mail: tangbenz@ust.hk

[b] H. Park, Prof. G. Niu, Dr. H. Zhang, Dr. R. T. K. Kwok, Dr. J. W. Y. Lam, Prof. B. Z. Tang
HKUST-Shenzhen Research Institute, No. 9 Yuexing 1st RD, South Area, Hi-tech Park, Nanshan, Shenzhen 518057, China

[c] Dr. S. Li, Dr. Z. Song, Prof. Q. Xiong
Clinical Medical College of Acupuncture Moxibustion and Rehabilitation, Mathematical Engineering Academy of Chinese Medicine, Guangzhou University of Chinese Medicine, Guangzhou 510006, China
E-mail: qpxiong@gmail.com

[d] Prof. G. Niu, Q. Lu, Prof. X. Yu
Center of Bio and Micro/Nano Functional Materials, State Key Laboratory of Crystal Materials, Shandong University, Jinan 250100, China

[e] C. Ma, Prof. K. S. Wong
Department of Physics, The Hong Kong University of Science and Technology, Clear Water Bay, Kowloon, Hong Kong 999077, China

[f] Prof. Q. Xiong
Jiangsu Key Laboratory of Regional Resource Exploitation and Medicinal Research, Faculty of Chemical Engineering, Huaiyin Institute of Technology, Huai'an 223003, Jiangsu, China
E-mail: qpxiong@gmail.com

[g] Prof. B. Z. Tang
Center for Aggregation-Induced Emission, SCUT-HKUST Joint Research Institute, State Key Laboratory of Luminescent Materials and Devices, South China University of Technology, Guangzhou 510640, China

[+] These authors contributed equally to this work.

Supporting information for this article is given via a link at the end of the document.

Abstract: Fatty liver disease (FLD) has become an increasing global health risk. However, an accurate diagnosis of FLD at an early stage remains a great challenge due to lack of suitable imaging tools. To this end, we developed the first fluorescent two-photon aggregation-induced emission (AIE) luminogen ABCXF for high-contrast imaging of FLD tissue. ABCXF has a large Stokes shift, good two-photon absorption cross-section, bright red emission, high fluorescence quantum yield in solid state, and excellent photostability. It shows abnormal intramolecular charge transfer effect instead of twisted intramolecular charge transfer effect in polar solvents. Photophysical and crystal data demonstrated that it exhibits nonaromatic rotors - trifluoromethyto contribute to its AIE effect. Biocompatible lipid droplet-targeting ABCXF can selectively light up lesions in the FLD tissue with a high signal-to-noise ratio. It shows superior imaging performances compared to Oil Red O. Thus, ABCXF can be a powerful tool for the diagnosis and evaluation of FLD from a liver biopsy.

Introduction

At present, human health is highly threatened by various kinds of diseases. Hepatic steatosis, commonly known as fatty liver disease (FLD), is a medical condition where excess lipid droplets accumulate in hepatocytes in the form of triglyceride.[1] It is categorized into two types: non-alcoholic fatty liver disease and alcoholic liver disease.[2] Recently, non-alcoholic FLD is receiving considerable attention as the prevalence of non-alcoholic FLD has increased to about 25% of the global population while no approved medication is available for the disease in the market.[3] Non-alcoholic FLD is known to be strongly associated with characteristics of metabolic syndromes, such as obesity, type-2 diabetes, dyslipidaemia and hypertension.[1, 4] An early stage of non-alcoholic FLD is reversible and managed through adjustment in diet and physical activities before progressing into more severe advanced stages including cirrhosis and hepatocellular carcinoma.[5] Therefore, an early diagnosis of FLD with a reliable detection method is paramount importance to the patients' prognostic outcome.

Several imaging-based methods have been developed for the diagnosis of FLD including computed tomography (CT), magnetic resonance imaging (MRI), and ultrasonography (US). However, CT requires a high level of exposure to X-ray radiation and MRI may be problematic for patients with uneven fatty change as it only allows them to evaluate a small sample volume.[6] The major downfall of the US is its high technical failure rate in morbidly obese patients.[7] All these methods also suffer from the low detection sensitivity. On the other hand, the ratio of the level of alanine transaminase (ALT) and aspartate transaminase (AST) which are important in the liver function, in blood may aid the diagnosis of FLD. Yet, as over 80% of the biochemistry remains normal, blood test based on the liver enzyme detection probably leads to patients remaining undiagnosed and untreated.[8, 9] Thus, it's in great demand for a simple and reliable detection technique for the examination of the liver condition.

In the modern clinical setting, diazo dyes such as Oil Red O are widely used for the diagnosis of FLD by histological staining of lipid droplets (LDs).[10] Unfortunately, the performance is rather unreliable. Apart from their unstable chemical structures and lack of selectivity toward LDs, the sample preparation using these dyes is extremely time-consuming, and the use of organic solvents like ethanol and isopropanol during the staining procedure due to their poor solubility may cause artificial fusion of LDs.[11] Furthermore, the shallow penetration in tissue fails to accurately visualize LDs via the conventional light microscopy.[12] Recently, fluorescence microscopy is widely utilized for

monitoring cell physiology and medical diagnosis due to its high sensitivity, selectivity, non-invasiveness and ability to provide excellent spatial and temporal resolution.[13-15] Two commercially available probes Nile Red and BODIPY493/503 are commonly used for LDs staining.[16] However, Nile Red suffers from high unspecific background fluorescence signal and broad emission peak which hinders its use in multi-color imaging. BODIPY493/503 exhibits small Stoke shifts to cause non-radiative energy loss and interference from the scattered light.[17, 18] Although some attempts have been made to develop new fluorescent probes for selective imaging of LDs,[19-21] fluorescent probes have been rarely utilized in the diagnosis of FLD due to their unsatisfying permeability, limited tissue penetration, and poor signal-to-noise ratio.[22] Generally, most of these reported probes usually work at low concentrations but their photostability by continuous irradiation especially high-intensity two-photon laser is under concern. On the other hand, increasing the concentration of the hydrophobic traditional dyes leads to unfavorable aggregation-caused quenching (ACQ) phenomenon.[23] Therefore, it is necessary and meaningful to develop ACQ-free and highly photostable fluorescent LD-specific probes for the diagnosis of FLD.

In 2001, our group coined the concept of aggregation-induced emission (AIE) which is the exact opposite of ACQ effect.[24] AIE luminogens (AIEgen) show non-emissive or weekly emissive in solutions but brightly emissive upon aggregation or in solid state through a mechanism of the restriction of intramolecular motions (RIM).[25, 26] Based on RIM, numerous AIEgens have been developed for various biological applications such as fluorescence imaging, biosensing, and disease diagnosis.[27-32] Compared with one-photon imaging, multiphoton like two-photon imaging using near-infrared excitation is more suitable in biomedical imaging because of the minimal background autofluorescence, low photobleaching, high spatial resolution, and deep tissue penetration.[33] Considering their high fluorescence brightness and photostability, AIEgens are naturally stable and promising candidates for two-photon imaging.[34-36] Since liver tissue suffers from the autofluorescence covering the whole visible light region, it would be ideal to develop a novel multiphoton-active AIEgen.[37] Conventionally, the introduction of the electron donor-acceptor (D-A) group into a π-conjugated system is a frequently used strategy to construct two-photon active fluorescent dyes.[38] Such a strategy generally results in intramolecular charge transfer (ICT), which is beneficial for enhancing the electron mobility and red-shifted and intensity-increased fluorescence. While most AIEgens show twisted intramolecular charge transfer (TICT) property rather than ICT effect, due to their highly twisted structures.[39] Pure TICT effect is detrimental for bioimaging because of the high polar water environment in biological system.[40] Therefore, the key to develop ICT-based AIEgens is to inhibit TICT effect in a D-A system by constructing a planar core. As the highly twisted AIEgens with numerous aromatic rings and rotors have the flexible cores, seeking some pendent nonaromatic rotors on the fluorescent planar cores probably leads to novel D-A based AIEgens with favorable ICT effect.

Recently, few potential bulky nonaromatic rotors have been reported.[41] Panigati et al. developed a TMS (Me_3Si) group substituted dinuclear rhenium complex with bright solid-state emissions of fluorescence quantum yield of over 50%, while it showed faint emission (fluorescence quantum yield of 6%) in toluene.[41a] The authors concluded that the intramolecular motions of the nonaromatic rotor of the TMS group quench the emission in solution and the restricted rotation of such nonaromatic rotor is most likely responsible for the boosted emission in crystals. Indeed, in our previous work, we observed an abnormal phenomenon of one trifluoroacetyl group replaced compound N-(2-((9*H*-fluoren-9-ylidene)(phenyl)methyl)phenyl)-2,2,2-trifluoroacetamide) with no emission in solution or aggregate state, which was completely AIE inactive.[41b] However, another acetyl group substituted compound N-(2-((9*H*-fluoren-9-ylidene)(phenyl)methyl)phenyl)acetamide was AIE active. We noticed that the trifluoromethyl group (CF_3) is also a nonaromatic rotor ascribed to the no emission of compound N-(2-((9*H*-fluoren-9-ylidene)(phenyl)methyl)phenyl)-2,2,2-trifluoroacetamide).
Based on this, we anticipated that the introduction of nonaromatic rotor CF_3 group could be a promising design strategy to maintain the good π-conjugation of AIEgens as well as favorable ICT effect. With these considerations in mind, we designed and synthesized a new donor and acceptor incorporated fluorescent two-photon compound ABCXF by decorating the nonaromatic rotor (CF_3) on the conjugated core. As we expected, single-crystal data indicates the planar structure of ABCXF. ABCXF is AIE-active and highly red-emissive in solid state. The abnormal ICT effect of this AIEgen was verified by investigating the fluorescence data in different polar solvents. Combined photophysical and crystal data revealed that nonaromatic rotors (CF_3) in ABCXF contribute to its AIE effect. Given its lipophilic structure, *in vitro* imaging data confirmed the high specificity of ABCXF in LDs. Compared with most LD dyes with complicated synthesis procedures, ABCXF was simply obtained via one-step synthesis. It was further utilized for the diagnosis of FLD obtained from guinea pig FLD tissues by one-photon and two-photon microscopy and the photostability of ABCXF under continuous one- and two-photon irradiation was investigated.

Results and Discussion

The synthesis route of ABCXF is depicted in Figure 1A. ABCXF was facilely obtained through a simple one-step nucleophilic reaction. Commercially available compound **1** and compound **2** were reacted in anhydrous EtOH in the presence of *t*-BuONa at 90 °C to yield ABCXF. ABCXF was characterized by ^{1}H NMR, ^{13}C NMR, ^{19}F NMR, and HRMS spectroscopy (Figures S1-S4). A detailed synthetic procedure was provided in the Supporting Information. The structure of ABCXF was confirmed by the single-crystal structure analysis (Figure 1B). It clearly shows that ABCXF almost exhibits a planar structure with a very small twisted angle of 10.55º between the trifluoromethyl substituted benzene plane and the other π-conjugated part of the molecule. The single crystal suitable for single-crystal analysis was obtained by slow evaporation of the solvent mixture of CH_2Cl_2 and MeOH (3:1, *v*/*v*) at room temperature. The details of the X-ray experimental conditions, cell data, and refinement data of ABCXF are summarized in Table S1. Additionally, DFT calculation was performed with the method of b3lyp/6-31g(d,p) by using the Gaussian 09 program package (Figure 1C).[42] The highest occupied molecular orbital (HOMO) was mostly delocalized on the other part of the molecule except for the trifluoromethylphenzene moiety, whereas the lowest unoccupied molecular orbital (LUMO) was delocalized on the

trifluoromethylphenyl substituted acrylonitrile unit. The energy bandgap between HOMO and LUMO was 2.92 eV. The D-A based ABCXF showed typical charge transfer characteristics as we expected.

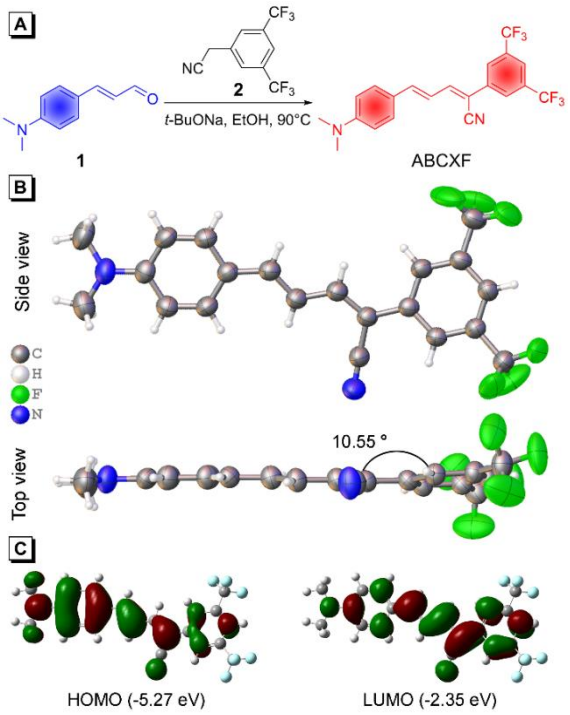

Figure 1. (A) Synthetic route of ABCXF. (B) ORTEP drawing of single crystal structure of ABCXF with atoms labelled in colour at different directions. CCDC 1904764. C, gray; H, white; F, green; N, blue. (C) Frontier molecular orbitals of ABCXF calculated with the method of b3lyp/6-31g(d,p) by using the Gaussian 09 program package, HOMO: highest occupied molecular orbital, LUMO: lowest unoccupied molecular orbital.

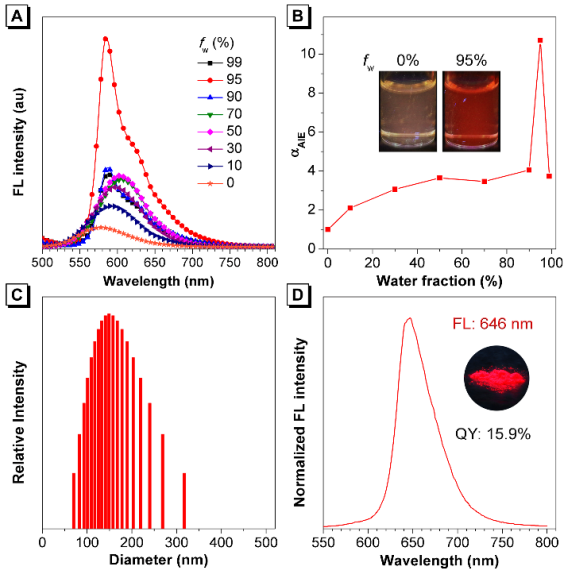

Figure 2. (A) FL spectra of ABCXF (10 μM) in THF/water mixtures with different water fractions (f_w). (B) The plot of FL emission intensity versus the composition of THF/water mixture containing ABCXF. Inset: fluorescent photographs of ABCXF in THF/water mixtures with different water fractions under 365 nm UV irradiation. (C) Dynamic light scattering data of ABCXF in water containing 5% of THF. Hydrated diameter: 154 nm. (D) Normalized FL spectra of amorphous ABCXF solid. Inset: fluorescent photograph of ABCXF taken under 365 nm UV irradiation.

We then systematically investigated its photophysical data. As shown in Figure S5, ABCXF possesses an absorption maximum (λ_{abs}) at 448 nm in THF which falls in the range of visible light allowing less photodamage to the biological system compared to UV light. The AIE property of ABCXF was studied in THF/water mixture with different water fractions (f_w) (Figure 2A, 2B, and S6). ABCXF shows an emission maximum (λ_{em}) at 579 nm in THF solution and a large Stokes shift of 131 nm. With the addition of water to the THF solution, its emission showed red shift and its intensity slightly increased as it reached f_w = 70%. At f_w = 95%, ABCXF showed the highest FL emission at 585 nm because of the formation of aggregates, indicating the aggregation-enhanced emission (AEE) property. A shoulder peak at about 605 nm also exists, due to different intermolecular interactions between ABCXF molecules in nanoaggregates. As water fraction further increased to 99%, the FL intensity drastically decreased. Such a phenomenon has been frequently reported and explained due to a change in morphology and size of nanoparticles at high water fraction.[25, 43] It is noteworthy that the ratio of FL increase at f_w= 95% compared to 0% is only 10 folds (Figure 2B), possibly indicating the formation of loose packing aggregates. The light dynamic scattering measurements show the presence of nanoaggregates in f_w = 95% and 99% with the size about 153 nm and 143 nm in diameter, respectively (Figure 2C and S7). ABCXF emits red-shifted emission (647 nm) in solid state compared with that in solution (Figure 2D). Before analyzing the intermolecular packing mode of ABCXF in the crystal to explain the red-shifted solid-state emission, we first recorded the X-ray diffraction (XRD) pattern of a pristine solid sample. As shown in Figure S8, its XRD pattern was very similar to the simulated XRD pattern from X-ray single crystal data, indicating the easy crystallization of ABCXF and similar interactions in pristine samples. Then, the intermolecular packing mode of ABCXF in the crystal was analyzed (Figure S9). It showed that some π···π interactions between the electron-donating and withdrawing groups, resulting in strong intermolecular D-A interactions and red-shifted emission in solid state. Generally, previously developed AIEgens possess highly twisted structures due to the presence of multiple aromatic rotors, and restriction of the movement of these rotors is known to be the cause of AIE phenomena. However, in the case of ABCXF, except for intermolecular C–H···π interactions, multiple intermolecular C–H···F interactions between adjacent molecules are also formed, indicating the motion inhibition of phenyl units and the CF_3 group. In addition, the disordered assembly of the CF_3 group attached to the phenyl could be observed (Figure S10),[44] further confirming the free motion of CF_3 groups in solution state but inhibited motion by crystal lattice in solid state. The restricted molecular motion of the nonaromatic rotor (CF_3 group) together with the aromatic rotors like phenyl group contributes to preventing the loss of excited-state energy via nonradiative decay channels, resulting in bright emission in solid state. After strong grinding of the solid ABCXF, the fluorescence showed only slight blue shift with a maximum wavelength of 625 nm (Figure S11), indicating stable intermolecular interactions. The absolute fluorescence quantum yield (QY) of ABCXF in solid state and diluted THF solution was measured using an integrating sphere. In the diluted THF solution, the fluorescence QY of

ABCXF is only 0.8 % as the active intramolecular motion consumed the energy of the excited state through non-radiative processes. However, in solid state, ABCXF is highly emissive with the fluorescence QY of 15.9 % due to restriction of intramolecular motion (Figure 2D).

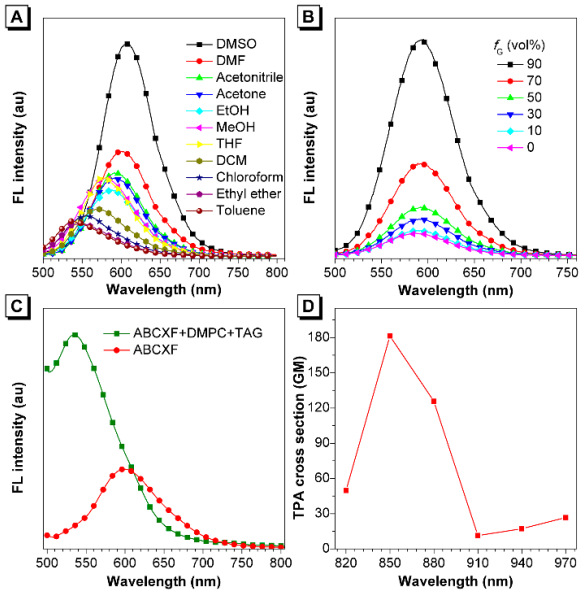

Figure 3. (A) FL spectra of ABCXF (10 μM) in different polar solvents. (B) FL spectra of ABCXF (5 μM) in methanol and methanol/glycerol mixture with different glycerol fractions (f_G). (C) FL spectra of ABCXF (1 μM) in PBS solution (pH= 7.2) with and without DMPC (40 μg/mL) and TAG (80 μg/mL). (D) Two-photon absorption (TPA) cross sections of ABCXF in THF. 1 GM= 10^{-50} cm^4s/photon.

As ABCXF is a donor-acceptor conjugated π-system, it is anticipated to display distinct fluorescence changes in different polar solvents. The λ_{em} of ABCXF gradually red-shifted from 550 to 620 nm with an increase in fluorescence intensity as the solvent polarity increased from toluene to DMSO (Figure 3A). The fluorescence QYs of ABCXF in different solvents were also recorded using an integrating sphere (Table S2). These interesting data together with the planar structure indicated that ABCXF shows positive solvatochromism in different polar solvents due to the ICT effect not TICT effect. Otherwise, the fluorescence intensity of ABCXF in high polar solvent like DMSO should greatly decrease. We further studied the effect of viscosity on ABCXF in glycerol/ MeOH mixture with different fractions of glycerol. As shown in Figure 3B, the fluorescence enhancement was observed as the viscosity of the solvent increased, which is also demonstrated the AIE effect of ABCXF. Given the lipophilicity of ABCXF with a calculated logP (n-octanol/water partition coefficient) value of 5.842, we anticipated that ABCXF probably is an LD-specific dye.[45] Therefore, we studied the photophysical property of ABCXF in the presence of 1,2-dimyristoyl-sn-glycero-3-phosphocholine (DMPC) and trioleate glycerol (TAG) in PBS to mimic the environment of LDs. The chemical structures of DMPC and TAG were displayed in Figure S12. As shown in Figure 3C, in the presence of key components of LDs, ABCXF displayed blue-shifted and enhanced fluorescence (about 3-fold) at about 525 nm compared to ABCXF only, which is beneficial for light-up fluorescence imaging in biological systems. By using the femtosecond pulse laser (800-1000nm) excited fluorescence and Rhodamine B as the standard,[46] we measured the two-photon absorption (TPA) cross section of ABCXF at different wavelengths. As displayed in Figure 3D, ABCXF has the maximum TPA cross section value of 180 GM at 850 nm. This result indicates that ABCXF is a good candidate to be utilized for two-photon fluorescence imaging.

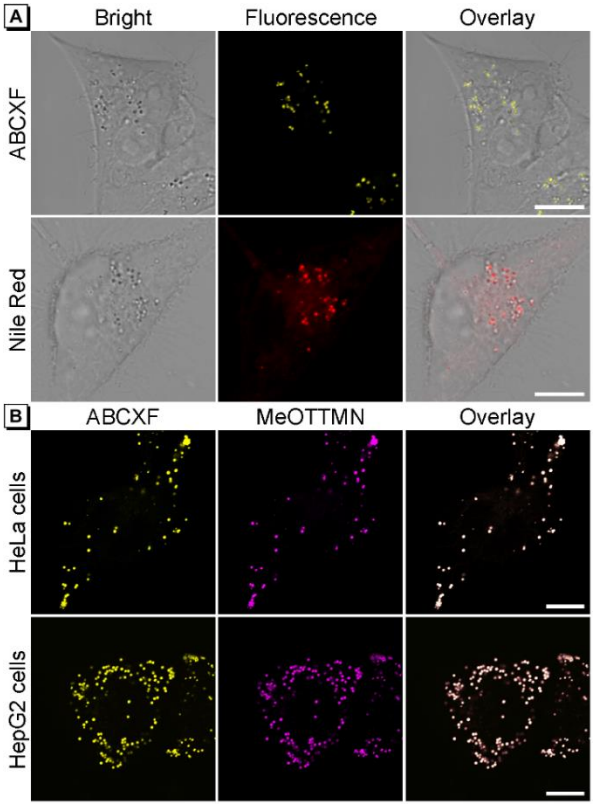

Figure 4. (A) Confocal laser scanning microscopy (λ_{ex} = 488 nm) images of HeLa cells stained with ABCXF (200 nM) and Nile Red (200 nM). Scale bar: 10 μm. (B) Confocal laser scanning microscopy (λ_{ex} = 488 nm) images of HeLa and HepG2 cells stained with ABCXF (200 nM) and MeOTTMN (2 μM). Scale bar: 10 μm.

Before evaluating its biological imaging applications, we first studied the cytotoxicity of ABCXF in HeLa and HepG2 cells by the standard MTT assay. Approximately 5000 cells were plated in each well of 96 well plate and after cells adhered to the plate surface, medium containing a range of concentration of ABCXF was added to each well. Over the range of concentration from 0.5 to 10 μM, ABCXF shows negligible cytotoxicity in both HeLa and HepG2 cells (Figure S13). Subsequently, live-cell imaging in HeLa and HepG2 cells were performed within the concentration range tested for the MTT assay by confocal laser scanning microscopy. After incubation of ABCXF at 200 nM for 20 min, bright spots in HeLa and HepG2 cells could be visualized with a high signal-to-noise ratio (Figures 4A and S14), probably indicating its location in LDs. However, the commercially available dye, Nile Red showed bright emission in LDs as well as non-specific fluorescence in the cytoplasm under the same condition, resulting in unsatisfying imaging contrast. The *in situ* fluorescence spectra of ABCXF in HeLa and HepG2 were acquired using the Lambda mode, and the data revealed that ABCXF exhibited blue-

shifted *in situ* fluorescence (about 550-555 nm) in live cells due to its ICT characteristic and the low polar environment of LDs (Figure S15). Considering the spectra overlap between ABCXF and Nile Red, we used another previously developed red/near-infrared probe MeOTTMN for co-stain experiments. As shown in Figure 4B, ABCXF showed excellent overlap with MeOTTMN with Pearson's coefficient value of 0.94 and 0.96 in HeLa and HepG2 cells, respectively. These data demonstrated that our AIEgen ABCXF is a suitable LD probe that works at an ultralow concentration of 200 nM for specific LDs staining with a high signal-to-noise ratio.

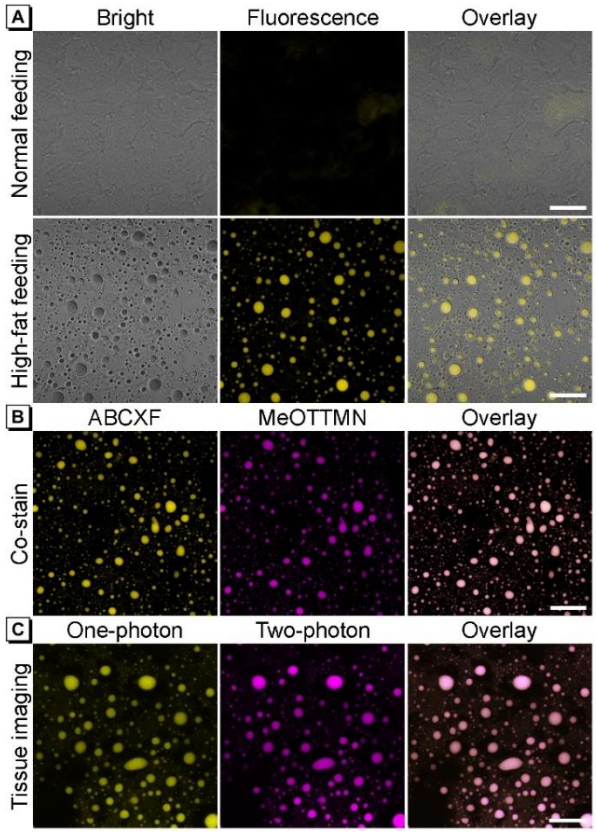

Figure 5. (A) One-photon (λ_{ex} = 488 nm) fluorescent images of normal and high-fat feeding guinea pig liver tissue stained with ABCXF (1 μM). Scale bar: 20 μm. (B) One-photon (λ_{ex} = 488 nm) fluorescent images of high-fat feeding guinea pig liver tissue stained with ABCXF (1 μM) and MeOTTMN (1 μM). Scale bar: 20 μm. (C) One-photon (λ_{ex} = 488 nm) and two-photon (λ_{ex} = 850nm) fluorescent images of high-fat feeding guinea pig liver tissue stained with ABCXF (1 μM). Scale bar: 20 μm.

As previous studies have shown that the hallmark of FLD is the excess lipid accumulation in the liver tissue.[1a, 47] ABXCF's ability to specifically stain LDs motivated us to investigate its ability to visualize LDs in lesions of the FLD tissue. We built a FLD model by providing a high-fat feeding diet to a group of male Hartley guinea pigs and as a control, a group of guinea pigs were fed with a normal diet under the same experimental conditions.[48] After five weeks of feeding, the livers were taken from the guinea pigs in both groups and the livers were sliced by a cryostat. The sectioned tissues were incubated with ABCXF for 1 h before the imaging. As predicted, ABCXF showed a strong yellow fluorescence in the FLD tissue from the high-fat feeding guinea pig (Figure 5A), due to its ICT effect and the viscous and low polar lipid environment (Figure 3C). Surprisingly, only very faint emission was collected in the control group because of the strong AIE effect. We performed co-stain experiment to confirm the staining location in lesions of the FLD tissue (Figure 5B). The data showed that ABCXF could specifically stain LDs with a high fluorescence overlap with that of MeOTTMN (Pearson's coefficient value of 0.92). Compared to previously developed two fluorescent probes for the FLD tissue imaging with the strong background fluorescence,[49, 19] ABCXF showed a highly improved signal-to-noise ratio. Such remarkable imaging contrast indicated that our LD-specific AIEgen ABCXF exhibit much potential in diagnosis of FLD.

Compared with one-photon fluorescence imaging, two-photon fluorescence imaging with a near-infrared excitation light is a promising imaging technique as the scattering coefficient is lower and the focus range is narrower, thus providing some outstanding advantages of deep tissue penetration, reduced photobleaching and lower phototoxicity.[50] Considering the good two-photon absorption cross-section (about 180 GM at 850 nm) of ABCXF, we carried out two-photon imaging of ABCXF in the FLD tissue. After incubation with ABCXF for 1 h, strong two-photon excited fluorescence signals in LDs were detected and showed a good overlap with one-photon excited fluorescence signals (Figure 5C). It should be noted that the two-photo[n fluorescence imaging displayed lower background fluorescence compared to the one-photon imaging.

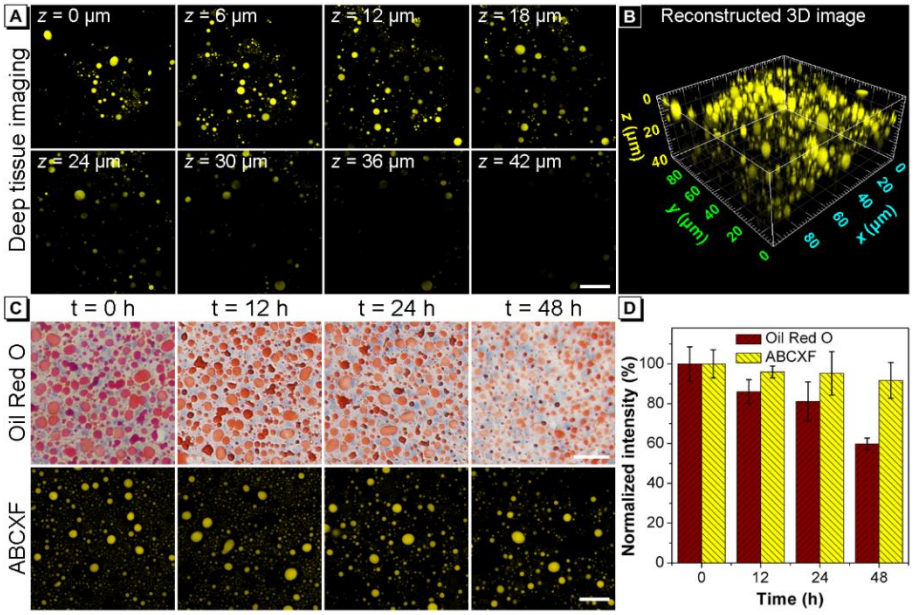

Figure 6. (A) Two-photon (λ_{ex} = 850 nm) fluorescent images of the high-fat feeding guinea pig liver tissue stained with ABCXF (2 μM) at different penetration depths. Scale bar: 20 μm. (B) Reconstructed 3D two-photon fluorescent images. (C) Bright-field and fluorescent images of the high-fat feeding guinea pig liver tissue stained with Oil Red O and ABCXF (1 μM), respectively, at different time points. Scale bar: 50 μm (Upper) or 20 μm (Lower). (D) Normalized color and fluorescence intensities obtained from images of the high-fat feeding guinea pig liver tissue stained with Oil Red O and ABCXF, respectively, at different time points.

One of the most outstanding merits of two-photon fluorescence imaging is that it enables deep penetration depth in tissue imaging. Considering the high-contrast two-photon imaging of ABCXF in lesions of 10 μm-thick FLD tissue, we investigated its penetration depth with a 100 μm-thick FLD tissue. The fluorescent images were captured every 3 μm along the *z*-axis. Under the excitation of 850 nm, the spherical LDs in the tissue sample were observed along the *z*-axis up to a depth of 42 μm (Figure 6A), and the 3D two-photon fluorescent image was successfully constructed with a high resolution (Figure 6B). However, compared to the two-photon imaging, the one-photon fluorescence imaging of ABCXF under 488 nm excitation only showed a shallow penetration depth of less than 30 μm along the *z*-axis (Figure S16). These data demonstrate that ABCXF can be used for visualization of LDs in lesions of the FLD tissue with a sufficient tissue penetration depth.

Oil Red O has been used for visualization of lipid and fat deposits in cell and tissue over the past decades under the bright-field microscopy. Especially, Oil Red O staining has been widely used as a histochemical stain for quantifying liver steatosis in liver biopsy samples. However, the Oil Red O staining method suffers from a low sensitivity and shallow tissue penetration compared to the fluorescence imaging method.[12, 51] Moreover, Oil Red O stained tissue must be analyzed within 24 h of staining due to its chemical instability and possible fusions of adjacent LDs.[11b] We stained the FLD tissue with Oil Red O and ABCXF separately to compare their imaging performances at the different time points of 0, 12, 24, and 48 h (Figure 6C and 6D). After 48 h of staining, the color of Oil Red O was dramatically faded and the intensity only remained 60% of the initial color intensity. However, the fluorescence intensity of ABCXF remained above 90% even after 48 h, demonstrating its superior tissue imaging performance over Oil Red O for the diagnosis of FLD.

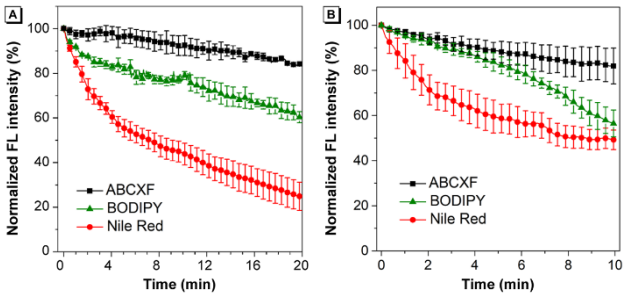

Figure 7. (A) One-photon photostability of ABCXF, Nile Red and BODIPY 493/503 under continuous irradiation (λ_{ex} = 488 nm for ABCXF and BODIPY 493/503, and 543 nm for Nile Red, laser power of 4 %) in HeLa cells. (B) Two-photon photostability of ABCXF, Nile Red, and BODIPY 493/503 under the same continuous irradiation (λ_{ex} = 850 nm) in the FLD tissues.

Encouraged by the desirable one- and two-photon imaging performance of ABCXF toward the visualization of LDs in lesions of the FLD tissue, we further studied its photostability under one-photon and two-photon excitations. First, we continuously irradiated HeLa cells stained with ABCXF (200 nM) with a 488-nm laser. Commercially available LD probes, Nile Red and BODIPY 493/503 were used as comparisons. As shown in Figure 7A, after continuous irradiation for 20 min, more than 80 % of the initial fluorescence of ABCXF intensity remained. Whereas, the fluorescence intensity of Nile Red and BODIPY 493/503 diminished to 59% and 22% of the initial fluorescence, respectively. We applied two-photon NIR excitation of 850 nm at the same continuous irradiation to further evaluate their photostability in the FLD tissue. It showed that ABCXF exhibits

higher photobleaching resistance than Nile Red and BODIPY 493/503 (Figure 7B). Previous works demonstrated that the trifluoromethyl substituted fluorescent dyes tend to have higher photostability compared to those of unsubstituted ones as the trifluoromethyl group contributes to an increase in oxidation potential and decrease in electron density, thereby reducing the probability of molecule being photobleached.[52,53] This explains why ABCXF exhibits a higher photostability under continuous one-photon and two-photon irradiation.

Conclusions

We successfully synthesized a novel AIEgen, ABCXF with unconventional nonaromatic rotors (CF_3) through a simple one-step nucleophilic reaction. ABCXF possesses favorable characteristics including a large Stokes shift (131 nm), good two-photon absorption cross-section (180 GM at 880 nm), bright red emission of 646 nm in the solid state (fluorescence quantum yield of 15.9 %). ABCXF showed ICT effect instead of TICT effect, which was revealed by the red-shifted and intensity-enhanced fluorescence of ABCXF in polar solvents. *In vitro* cell imaging data confirmed the specific staining property of ABCXF in LDs at an ultralow incubation concentration (200 nM). Due to its ICT effect and non-polar and viscous environment of LDs, ABCXF displayed blue-shifted and intensity-enhanced fluorescence in LDs and greatly increased its emission in lesions of FLD tissue. As ABCXF is comprised of an electron-donor and acceptor in a conjugated π-system, it was utilized for the two-photon fluorescent imaging with a high signal-to-noise ratio and satisfying tissue penetration depth of 42 μm. Moreover, ABCXF exhibits better performance compared to clinically used diazo dye, Oil Red O in terms of the staining procedure, sensitivity, penetration depth, and chemical stability and shows remarkably higher photobleaching resistance under continuous one- and two-photon irradiation compared to commercial LD probes, Nile Red and BODIPY 493/503. We expect ABCXF can be a possible replacement of pre-existing LD probes for the diagnosis of FLD. Our design strategy can potentially serve as a guidance for the development of other new fluorescent systems with nonaromatic rotors and this work opens new avenues for the use of ICT effect instead of TICT effect to construct bright NIR-emissive fluorescent dyes for *in vivo* biomedical imaging.

Acknowledgements

This work was partially supported by the National Basic Research Program of China (21788102), the University Grants Committee of Hong Kong (AoE/P-02/12), the Research Grants Council of Hong Kong (16305518, N_HKUST609/19 and C6009-17G), the Innovation and Technology Commission (ITC-CNERC14SC01 and ITCPD/17-9), the Science and Technology Plan of Shenzhen (JCYJ20170818113851132, JCYJ20170818113840164, and JCYJ20180507183832744), the Special Fund of Taishan Scholars Project of Shandong Province, China (tsqn201909012), the Opening Fund of Key Laboratory of Photochemical Conversion and Optoelectronic Materials, TIPC, CAS (PCOM202001), and the Program of Qilu Young Scholars of Shandong University.

Keywords: Aggregation-induced emission, nonaromatic rotor, multiphoton, diagnosis, fatty liver disease, lipid droplet

References

[1] a) P. Angulo, *N. Engl. J. Med.* **2002**, *346*, 1221-1231; b) F. Nassir, R. S. Rector, G. M. Hammoud, J. A. Ibdah, *Gastroenterol Hepatol.* **2015**, *11*, 167-175.
[2] N. Chalasani, Z. Younossi, J. E. Lavine, A. M. Diehl, E. M. Brunt, K. Cusi, M. Charlton, A. J. Sanyal, *Hepatology* **2012**, *55*, 2005-2023.
[3] a) Z. M. Younossi, A. B. Koenig, D. Abdelatif, Y. Fazel, L. Henry, M. Wymer, *Hepatology* **2016**, *64*, 73-84; b) B. A. Neuschwander-Tetri, *BMC Med.* **2017**, *15*, 45.
[4] F. A. Romero, C. T. Jones, Y. Xu, M. Fenaux, R. L. Halcomb, *J. Med. Chem.* **2020**, *63*, 5031-5073.
[5] A. M. Diehl, C. Day, *N. Engl. J. Med.* **2017**, *377*, 2063-2072.
[6] a) D. H. Lee, *Clin. Mol. Hepatol.* **2017**, *23*, 290-301; b) N. Stefan, H.-U. Häring, K. Cusi, *Lancet Diabetes Endo.* **2019**, *7*, 313-324.
[7] C. C. Mottin, M. Moretto, A. V. Padoin, A. M. Swarowsky, M. G. Toneto, L. Glock, G. Repetto, *Obes. Surg.* **2004**, *14*, 635-637.
[8] N. M. de Alwis, Q. M. Anstee, C. P. Day, *Dig. Dis.* **2016**, *34* Suppl 1, 19-26.
[9] M. Bayard, J. Holt, E. Boroughs, *Am. Fam. Physician* **2006**, 73, 1961-1968.
[10] R. Koopman, G. Schaart, M. K. Hesselink, *Histochem Cell. Biol.* **2001**, *116*, 63-68.
[11] a) T. Fujimoto, Y. Ohsaki, J. Cheng, M. Suzuki, Y. Shinohara, *Histochem. Cell Biol.* **2008**, *130*, 263-279; b) S. Fukumoto, T. Fujimoto, *Histochem Cell Biol* **2002**, *118*, 423-428.
[12] A. Mehlem, C. E. Hagberg, L. Muhl, U. Eriksson, A. Falkevall, *Nat. Protocols* **2013**, *8*, 1149-1154.
[13] a) R. Yuste, *Nat. Methods* **2005**, *2*, 902-904; b) H. Li, Q. Yao, F. Xu, Y. Li, D. Kim, J. Chung, G. Baek, X. Wu, P. F. Hillman, E. Y. Lee, H. Ge, J. Fan, J. Wang, S. J. Nam, X. Peng, J. Yoon, *Angew. Chem.* **2020**, *132*, 10272-10281; *Angew. Chem. Int. Ed.* **2020**, *59*, 10186-10195.
[14] Z. Wu, M. Liu, Z. Liu, Y. Tian, *J. Am. Chem. Soc.* **2020**, *142*, 7532-7541.
[15] W. Xu, Z. Zeng, J. H. Jiang, Y. T. Chang, L. Yuan, *Angew. Chem.* **2016**, *128*, 13858-13902; *Angew. Chem. Int. Ed.* **2016**, *55*, 13658-13699.
[16] T. K. Fam, A. S. Klymchenko, M. Collot, *Materials* **2018**, *11*, 1768.
[17] P. Greenspan, E. P. Mayer, S. D. Fowler, *J. Cell Biol.* **1985**, *100*, 965-973.
[18] Y. Ohsaki, Y. Shinohara, M. Suzuki, T. Fujimoto, Histochem. *Cell Biol.* **2010**, *133*, 477-480.
[19] L. Guo, M. Tian, R. Feng, G. Zhang, R. Zhang, X. Li, Z. Liu, X. He, J. Z. Sun, X. Yu, *ACS Appl. Mater. Interfaces* **2018**, *10*, 10706-10717.
[20] X. Zheng, W. Zhu, F. Ni, H. Ai, S. Gong, X. Zhou, Jonathan L. Sessler, C. Yang, *Chem. Sci.* **2019**, *10*, 2342-2348.
[21] M. Collot, T. K. Fam, P. Ashokkumar, O. Faklaris, T. Galli, L. Danglot, A. S. Klymchenko, *J. Am. Chem. Soc.* **2018**, *140*, 5401-5411.
[22] a) C. A. Bader, R. D. Brooks, Y. S. Ng, A. Sorvina, M. V. Werrett, P. J. Wright, A. G. Anwer, D. A. Brooks, S. Stagni, S. Muzzioli, M. Silberstein, B. W. Skelton, E. M. Goldys, S. E. Plush, T. Shandala, M. Massi, *RSC Adv.* **2014**, *4*, 16345-16351; b) A. Wu, J. L. Kolanowski, B. B. Boumelhem, K. Yang, R. Lee, A. Kaur, S. T. Fraser, E. J. New, L. M. Rendina, *Chem. Asian J.* **2017**, *12*, 1704-1708.
[23] M. Gao, H. Su, S. Li, Y. Lin, X. Ling, A. Qin, B. Z. Tang, *Chem. Commun.* **2017**, *53*, 921-924.
[24] J. Luo, Z. Xie, J. W. Lam, L. Cheng, H. Chen, C. Qiu, H. S. Kwok, X. Zhan, Y. Liu, D. Zhu, B. Z. Tang, *Chem. Commun.* **2001**, 1740-1741.
[25] J. Mei, N. L. Leung, R. T. Kwok, J. W. Lam, B. Z. Tang, *Chem. Rev.* **2015**, *115*, 11718-11940.
[26] Y. Hong, J. W. Lam, B. Z. Tang, *Chem. Soc. Rev.* **2011**, *40*, 5361-5388.
[27] a) J. Qian, B. Z. Tang, *Chem* **2017**, *3*, 56-91; b) Z. Guo, C. Yan, W. H. Zhu, *Angew. Chem.* **2020**, *132*, 9896-9909; *Angew. Chem. Int. Ed.* **2020**, *59*, 9812-9825.
[28] T. C. Owyong, P. Subedi, J. Deng, E. Hinde, J. J. Paxman, J. M. White, W. Chen, B. Heras, W. W. H. Wong, Y. Hong, *Angew. Chem.* **2020**, *132*, 10215-10221; *Angew. Chem. Int. Ed.* **2020**, *59*, 10129-10135.
[29] W. Chi, J. Chen, W. Liu, C. Wang, Q. Qi, Q. Qiao, T. M. Tan, K. Xiong, X. Liu, K. Kang, Y.-T. Chang, Z. Xu, X. Liu, *J. Am. Chem. Soc.* **2020**, *142*, 6777-6785.

[30] a) X. He, L.-H. Xiong, Y. Huang, Z. Zhao, Z. Wang, J. W. Y. Lam, R. T. K. Kwok, B. Z. Tang, *TrAC Trend. Anal. Chem.* **2020**, 122, 115743; bB. He, B. Situ, Z. Zhao, L. Zheng, *Small Methods* **2020**, *4*, 1900583.
[31] F. Xia, J. Wu, X. Wu, Q. Hu, J. Dai, X. Lou, *Acc. Chem. Res.* **2019**, *52*, 3064-3074.
[32] X. Zhu, J.-X. Wang, L.-Y. Niu, Q.-Z. Yang, *Chem. Mater.* **2019**, *31*, 3573-3581.
[33] a) W. Qin, N. Alifu, J. W. Y. Lam, Y. Cui, H. Su, G. Liang, J. Qian, B. Z. Tang, *Adv. Mater.* **2020**, *32*, 2000364; b) N. Hamon, A. Roux, M. Beyler, J.-C. Mulatier, C. Andraud, C. Nguyen, M. Maynadier, N. Bettache, A. Duperray, A. Grichine, S. Brasselet, M. Gary-Bobo, O. Maury, R. Tripier, *J. Am. Chem. Soc.* **2020**, *142*, 10184-10197; c) X. Lou, Z. Zhao, B. Z. Tang, Small 2016, 12, 6430-6450; d) Y. Wang, M. Chen, N. Alifu, S. Li, W. Qin, A. Qin, B. Z. Tang, J. Qian, *ACS Nano* **2017**, *11*, 10452-10461.
[34] G. Niu, R. Zhang, J. P. C. Kwong, J. W. Y. Lam, C. Chen, J. Wang, Y. Chen, X. Feng, R. T. K. Kwok, H. H. Y. Sung, I. D. Williams, M. R. J. Elsegood, J. Qu, C. Ma, K. S. Wong, X. Yu, B. Z. Tang, *Chem. Mater.* **2018**, *30*, 4778-4787.
[35] M. Jiang, X. Gu, J. W. Y. Lam, Y. Zhang, R. T. K. Kwok, K. S. Wong, B. Z. Tang, *Chem. Sci.* **2017**, *8*, 5440-5446.
[36] W. Zhuang, L. Yang, B. Ma, Q. Kong, G. Li, Y. Wang, B. Z. Tang, *ACS Appl. Mater. Interfaces* **2019**, *11*, 20715-20724.
[37] a) A. C. Croce, A. Ferrigno, G. Bottiroli, M. Vairetti, *Liver Int.* **2018**, *38*, 1160-1174; b) A. C. Croce, A. Ferrigno, G. Santin, V. M. Piccolini, G. Bottiroli, M. Vairetti, *Lasers Surg. Med.* **2014**, *46*, 412-421.
[38] S. Singha, D. Kim, B. Roy, S. Sambasivan, H. Moon, A. S. Rao, J. Y. Kim, T. Joo, J. W. Park, Y. M. Rhee, T. Wang, K. H. Kim, Y. H. Shin, J. Jung, K. H. Ahn, *Chem. Sci.* **2015**, *6*, 4335-4342.
[39] a) Y. Li, Z. Cai, S. Liu, H. Zhang, S. T. H. Wong, J. W. Y. Lam, R. T. K. Kwok, J. Qian, B. Z. Tang, *Nat. Commun.* **2020**, *11*, 1255; b) S. Sasaki, G. P. C. Drummen, G.-i. Konishi, *J. Mater. Chem. C* **2016**, *4*, 2731-2743.
[40] a) J. B. Grimm, B. P. English, J. Chen, J. P. Slaughter, Z. Zhang, A. Revyakin, R. Patel, J. J. Macklin, D. Normanno, R. H. Singer, T. Lionnet, L. D. Lavis, *Nat. Methods* **2015**, *12*, 244-250; b) X. Liu, Q. Qiao, W. Tian, W. Liu, J. Chen, M. J. Lang, Z. Xu, *J. Am. Chem. Soc.* **2016**, *138*, 6960-6963.
[41] a) E. Quartapelle Procopio, M. Mauro, M. Panigati, D. Donghi, P. Mercandelli, A. Sironi, G. D'Alfonso, L. De Cola, *J. Am. Chem. Soc.* **2010**, *132*, 14397-14399; b) H. Tong, Y. Dong, Y. Hong, M. Häussler, J. W. Y. Lam, H. H. Y. Sung, X. Yu, J. Sun, I. D. Williams, H. S. Kwok, B. Z. Tang, *J. Phys. Chem. C* **2007**, *111*, 2287-2294.
[42] M. J. Frisch, G. W. Trucks, H. B. Schlegel, G. E. Scuseria, M. A. Robb, J. R. Cheeseman, G. Scalmani, V. Barone, G. A. Petersson, H. Nakatsuji, X. Li, M. Caricato, A. V. Marenich, J. Bloino, B. G. Janesko, R. Gomperts, B. Mennucci, H. P. Hratchian, J. V. Ortiz, A. F. Izmaylov, J. L. Sonnenberg, Williams, F. Ding, F. Lipparini, F. Egidi, J. Goings, B. Peng, A. Petrone, T. Henderson, D. Ranasinghe, V. G. Zakrzewski, J. Gao, N. Rega, G. Zheng, W. Liang, M. Hada, M. Ehara, K. Toyota, R. Fukuda, J. Hasegawa, M. Ishida, T. Nakajima, Y. Honda, O. Kitao, H. Nakai, T. Vreven, K. Throssell, J. A. Montgomery Jr., J. E. Peralta, F. Ogliaro, M. J. Bearpark, J. J. Heyd, E. N. Brothers, K. N. Kudin, V. N. Staroverov, T. A. Keith, R. Kobayashi, J. Normand, K. Raghavachari, A. P. Rendell, J. C. Burant, S. S. Iyengar, J. Tomasi, M. Cossi, J. M. Millam, M. Klene, C. Adamo, R. Cammi, J. W. Ochterski, R. L. Martin, K. Morokuma, O. Farkas, J. B. Foresman, D. J. Fox, Wallingford, CT, **2016**.
[43] T. Han, Y. Hong, N. Xie, S. Chen, N. Zhao, E. Zhao, J. W. Y. Lam, H. H. Y. Sung, Y. Dong, B. Tong, B. Z. Tang, *J. Mater. Chem. C* **2013**, *1*, 7314-7320.
[44] J. Zhang, X. Ma, X. Xuan, *Chinese J. Struct. Chem* **2020**, *39*, 698-708.
[45] R. W. Horobin, F. Rashid-Doubell, J. D. Pediani, G. Milligan, *Biotech. Histochem.* **2013**, *88*, 440-460.
[46] N. S. Makarov, M. Drobizhev, A. Rebane, *Opt. Express* **2008**, *16*, 4029-4047.
[47] E. Fabbrini, S. Sullivan, S. Klein, *Hepatology* **2010**, *51*, 679-689.
[48] G. Barja, M. Lopez-Torres, R. Perez-Campo, C. Rojas, S. Cadenas, J. Prat, R. Pamplona, *Free Radic. Biol. Med.* **1994**, *17*, 105-115.
[49] T. Shao, T. Liu, H. Liu, M. Zhang, Y. Shen, A. Gao, X. Tian, Q. Zhang, J. Wu, Y. Tian, *J. Mater. Chem. B* **2019**, *7*, 3704-3709.
[50] a) F. Helmchen, W. Denk, *Nat. Methods* **2005**, *2*, 932-940; b) M. Collot, P. Ashokkumar, H. Anton, E. Boutant, O. Faklaris, T. Galli, Y. Mely, L. Danglot, A. S. Klymchenko, *Cell Chem. Biol.* **2019**, *26*, 600-614 e607; c) K. Svoboda, R. Yasuda, *Neuron* **2006**, *50*, 823-839; d) M. Pawlicki, H. A. Collins, R. G. Denning, H. L. Anderson, *Angew. Chem.* **2020**, *121*, 3292-3316; *Angew. Chem. Int. Ed.* **2009**, *48*, 3244-3266.
[51] K. Si, R. Fiolka, M. Cui, *Sci. Rep.* **2012**, *2*, 748.
[52] S. Choi, J. Bouffard, Y. Kim, *Chem. Sci.* **2014**, *5*, 751-755.
[53] a) G. Y. Mitronova, V. N. Belov, M. L. Bossi, C. A. Wurm, L. Meyer, R. Medda, G. Moneron, S. Bretschneider, C. Eggeling, S. Jakobs, S. W. Hell, *Chem. Eur. J.* **2010**, *16*, 4477-4488; b) Y. Xing, C. Liu, X. Song, J. Li, *J. Mater. Chem. C* **2015**, *3*, 2166-2174.

Table of Contents

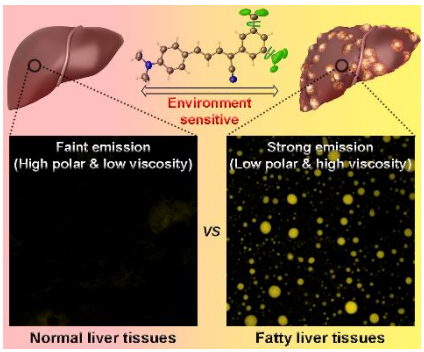

We present the first two-photon AIEgen ABCXF with nonaromatic rotors (CF_3) for fatty liver disease (FLD) diagnosis. ABCXF shows high two-photon absorption cross-section, bright red emission in solid state, and remarkably high photostability. The environment sensitive ABCXF can selectively light up FLD tissues with high contrast. Deep-tissue visualization of lipid droplets in the FLD tissue is also achieved under two-photon microscopy.